Original Article

Assessing colitis *ex vivo* using optical coherence elastography in a murine model

Achuth Nair[1], Chih Hao Liu[1], Manmohan Singh[1], Susobhan Das[1], Triet Le[1], Yong Du[1], Sanam Soomro[1], Salavat Aglyamov[2,3], Chandra Mohan[1], Kirill V. Larin[1]

[1]Department of Biomedical Engineering, [2]Department of Mechanical Engineering, University of Houston, Houston, TX, USA; [3]Department of Biomedical Engineering, University of Texas at Austin, Austin, TX, USA

Correspondence to: Chandra Mohan; Kirill V. Larin. Department of Biomedical Engineering, University of Houston, Houston, TX, USA. Email: cmohan@central.uh.edu; klarin@central.uh.edu.

Background: Ulcerative colitis (UC) is an inflammatory bowel disease (IBD) that causes regions of ulceration within the interior of the colon. UC is estimated to afflict hundreds of thousands of people in the United States alone. In addition to traditional colonoscopy, ultrasonic techniques can detect colitis, but have limited spatial resolution, which frequently results in underdiagnoses. Nevertheless, clinical diagnosis of colitis is still generally performed via colonoscopy. Optical techniques such as confocal microscopy and optical coherence tomography (OCT) have been proposed to detect UC with higher resolution. However, UC can potentially alter tissue biomechanical properties, providing additional contrast for earlier and potentially more accurate detection. Although clinically available elastography techniques have been immensely useful, they do not have the resolution for imaging small tissues, such as in small mammalian disease models. However, OCT-based elastography, optical coherence elastography (OCE), is well-suited for imaging the biomechanical properties of small mammal colon tissue.

Methods: In this work, we induced elastic waves in *ex vivo* mouse colon tissue using a focused air-pulse. The elastic waves were detected using a phase-stabilized swept source OCE system, and the wave velocity was translated into stiffness. Measurements were taken at six positions for each sample to assess regional sample elasticity. Additional contrast between the control and diseased tissue was detected by analyzing the dispersion of the elastic wave and tissue optical properties obtained from the OCT structural image.

Results: The results show distinct differences ($P<0.05$) in the stiffness between control and colitis disease samples, with a Young's modulus of 11.8±8.0 and 5.1±1.5 kPa, respectively. The OCT signal standard deviations for control and diseased samples were 5.8±0.3 and 5.5±0.2 dB, respectively. The slope of the OCT signal spatial frequency decay in the control samples was 92.7±10.0 and 87.3±4.7 dB·μm in the colitis samples. The slope of the linearly fitted dispersion curve in the control samples was 1.5 mm, and 0.8 mm in the colitis samples.

Conclusions: Our results show that OCE can be utilized to distinguish tissue based on stiffness and optical properties. Our estimates of tissue stiffness suggest that the healthy colon tissue was stiffer than diseased tissue. Furthermore, structural analysis of the tissue indicates a distinct difference in tissue optical properties between the healthy and UC-like diseased tissue.

Keywords: Inflammatory bowel diseases (IBDs); ulcerative colitis (UC); optical coherence tomography (OCT); optical coherence elastography (OCE); elasticity imaging techniques; tissue biomechanical properties

Submitted Feb 26, 2019. Accepted for publication May 30, 2019.
doi: 10.21037/qims.2019.06.03
View this article at: http://dx.doi.org/10.21037/qims.2019.06.03

Introduction

Ulcerative colitis (UC) is an inflammatory bowel disease (IBD) that manifests as large regions of continuous ulcerations throughout the inner lining of the colon (1). UC has an estimated prevalence of 238 cases out of every 100,000 people in the United States (1). The burden of illness for UC is quite high as it is associated with drastic decreased quality of life and significant morbidity. Furthermore, meta-analysis suggests a colorectal cancer prevalence of 3.7% in patients that already have UC (2). Due to significant public health efforts, including increasing awareness of the adverse effects of smoking, promoting screening such as colonoscopies above the age of 50, and more effective therapies, the incidence and mortality due to IBDs such as UC have decreased significantly (3). Despite the overall success in detecting and managing IBDs, research has shown that the incidence of pediatric IBDs, including UC, is on the rise internationally (4). This suggests that additional screening techniques, detection methods, and therapies are still needed to combat IBD.

Currently, the diagnosis of UC is performed using a combination of methods, including blood tests, stool tests, and colonoscopy. While blood and stool tests can provide helpful information, they are not definite methods to identify IBD. Physicians can use colonoscopy to visually identify inflammation and ulceration in the colon symptomatic of UC. However, colonoscopy is inherently limited to structural imaging and cannot provide depth-resolved information (5). Ultrasonic imaging has been proposed to detect UC, but has limited spatial resolution and cannot detect micrometer-scale changes in tissue properties (6,7). Optical techniques, such as endoscopic optical coherence tomography (OCT), have also been proposed to detect IBD with superior spatial resolution and depth resolved imaging (8-11). Similar to other structural imaging modalities, the diagnostic relevance of OCT is limited without a robust, quantifiable metric to distinguish control and diseased tissue. Histological analysis of biopsy tissue provides a method for directly assessing tissue health, however a faster and noninvasive alternative to detect diseased tissue would be a powerful clinical tool.

Elastography is a well-established technique to image mechanical contrast in tissue by using an imaging modality, such as ultrasound or magnetic resonance imaging, to detect displacements in tissue. Ultrasound elastography and magnetic resonance elastography are clinically available techniques that have been immensely useful at detecting diseases, such as cirrhosis, cancer, and sclerosis, among others (12). More specifically, magnetic resonance elastography and ultrasound elastography have been used to distinguish gastroenterological pathologies such as UC, but both methods are limited by the resolution of their parent imaging modality and require large amplitude displacements for accurate detection, which may not be suitable to detect small lesions and small mammal samples (13-15). It has been repeatedly shown that screening and early detection are vital to achieving positive patient outcome, so identifying tissue anomalies early using high resolution techniques is needed for effective disease management.

Optical coherence elastography (OCE) is an elastographic technique that utilizes OCT to image tissue motion (16). The parent imaging modality, OCT, can be used to capture microscopic displacements in tissue, enabling high resolution imaging of mechanical contrast (17). However, the elastographic resolution is based on the excitation technique, biomechanical reconstruction method, and mechanical contrast (18). In general, OCE benefits from higher resolution than alternative elastography methods that have been employed for characterizing colorectal pathologies (14,15). Endoscopic OCT has been used to image colorectal pathologies in humans (11). However, to the best of our knowledge, OCE has never been used to assess colorectal tissue.

During OCE imaging, the OCT image is captured. Thus, combined analyses of structural and biomechanical properties can enable more robust assessment of tissue health (19). This dual pronged method of tissue analysis could potentially be an effective supplemental clinical tool, which can be useful for assessing tissue mechanical properties and identifying disease margins with no contact with the sample. In this work, air-pulse OCE was used to assess the optical and mechanical properties of control and Dextran Sulfate Sodium-induced colitis, in *ex vivo* murine colons (20). Shear wave imaging OCE (SWI-OCE) measurements were performed to assess overall sample biomechanical properties based on the air-pulse induced elastic wave (21). Analysis of the dispersive behavior of the elastic wave provides another parameter for differentiating control and diseased tissue (22). Furthermore, analysis of the OCT structural image was utilized to distinguish healthy and diseased samples based on tissue optical properties. Combined optical and biomechanical parameters were used to detect the diseased tissue in single-blind measurements. The data demonstrate that OCE can successfully detect colitis and may be useful as a supplemental clinical tool to distinguish control and UC-diseased tissue.

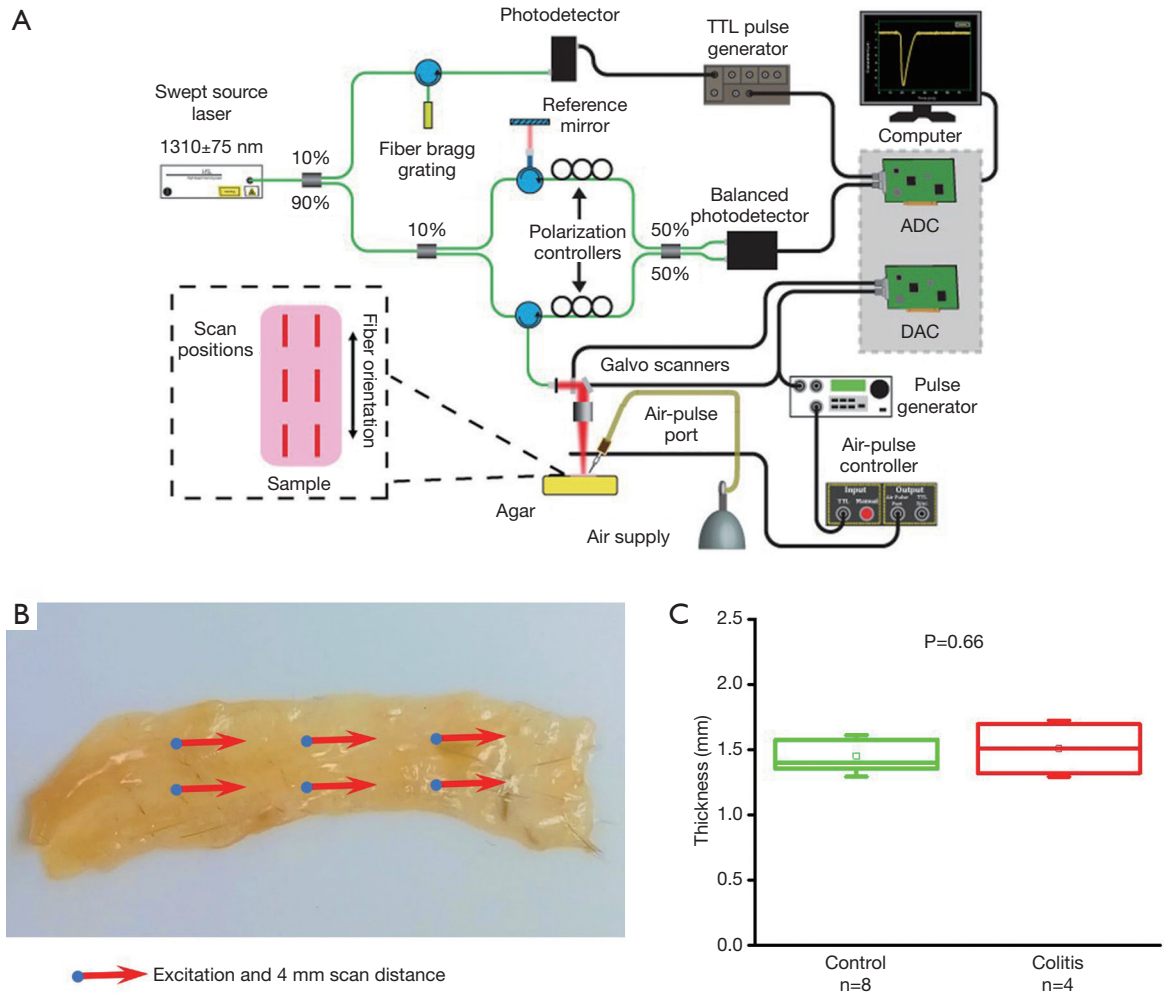

Figure 1 Schematic and OCE measurement. (A) Shows the schematic of the PhS-SSOCE system used to obtain optical and elastic measurements on the colon samples. The excitation and measurement procedure on a colon sample is shown in (B). Note that excitation (blue) is performed at the leftmost position of the scan and images are taken along the propagation path (red) to determine velocity. Markers are not drawn to scale. (C) Shows the thickness of the colon tissue, grouped accordingly after samples were unblinded. OCE, optical coherence elastography.

Methods

Murine colon specimens extracted from thirteen samples were subject to OCE measurements. Samples were tested in a single blind experiment—the health of the tissue was not known prior to OCE imaging so that testing remained unbiased. Colitis was induced in mice using a well-documented dextran sulfate sodium (DSS) protocol (20,23). The animals were euthanized, and the colons were extracted for analysis and OCE imaging. The colon samples were dissected and carefully spread on a 1% (w/w) nutrient agar phantom (Difco nutrient agar, Becton, Dickinson and Company). Each dissected colon sample was approximately rectangular, ~1.5 mm in thickness, ~8 mm in width, and ~20 mm in length, with no relationship between dimension and sample type, as shown in *Figure 1*. 1X phosphate buffered saline (PBS) was regularly applied to maintain its hydration state. Measurements of optical and mechanical properties were taken at six positions for each sample along the length of the colon, and the average measurement was utilized to characterize the sample.

OCE measurements were performed with a phase-stability swept source OCE (PhS-SSOCE) system that has been described in our previous work (24). A focused micro

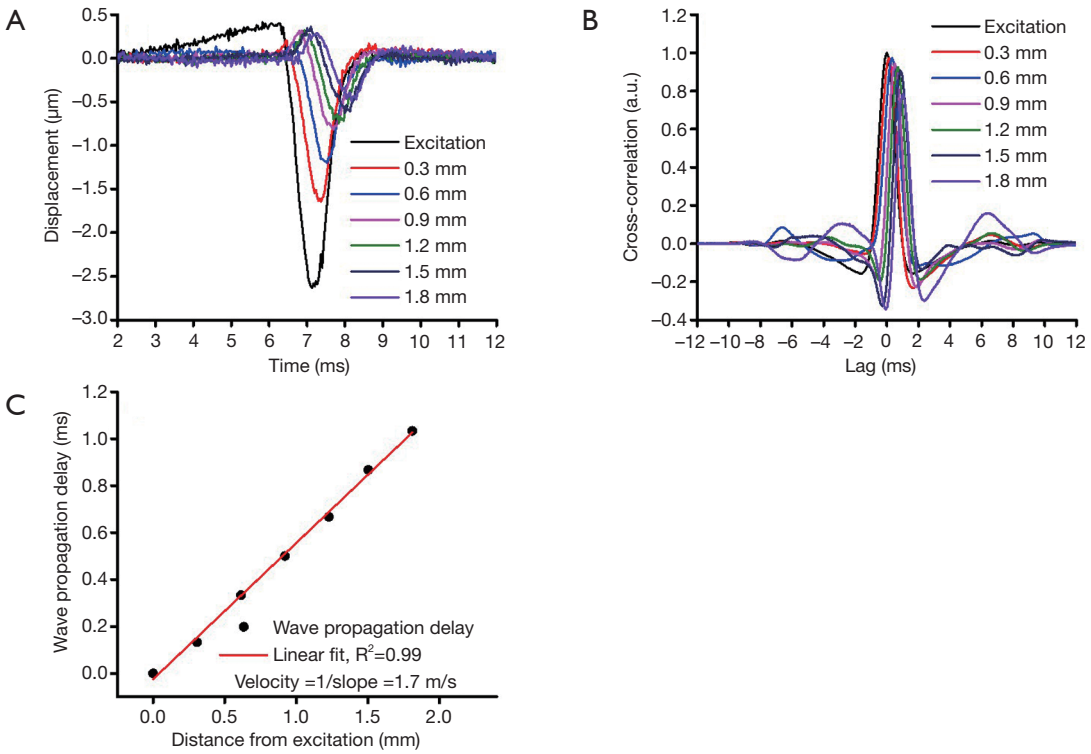

Figure 2 Group velocity calculation of the elastic wave. *Figure 2* shows the calculation of the elastic wave group velocity. The vertical temporal displacement profiles (A) from each successive position were cross-correlated with the displacement profile from the excitation position (B). The elastic wave propagation delay was determined from the maximum of the cross-correlation, and the velocity was obtained from the slope of a linear fit of the elastic wave propagation delays to the corresponding propagation distances (C).

air-pulse was synchronized to the OCT system, which consisted of a swept source laser (HSL2000, Santec Inc., Hackensack, NJ), with a 30 kHz sweep rate, 16 μm lateral resolution, and 11 μm axial resolution. A short duration (≤1 ms) focused micro air-pulse (25) induced low amplitude elastic waves (<10 μm), which were imaged by the OCT system. The OCE system schematic, experimental setup, and sample thickness are shown in *Figure 1*.

The elastic wave was imaged via 251 successive equidistant M-mode OCT images along a scan region of ~4 mm (21). Each M-mode OCT image was 1,500 A-line long, corresponding to 50 ms. Velocity calculation has been detailed in our previous work, and is summarized in *Figure 2* (26). First, the raw OCT phase profiles were unwrapped and converted to displacement and corrected for the motion of the surface and difference in refractive index between the air and tissue surface (27). The velocity of the elastic wave was determined by linearly fitting the wave propagation distances to the corresponding wave propagation delays (28). Wave propagation was shown only over 2 mm in *Figure 2* as an example. The delays were determined by cross-correlation analysis. The temporal displacement profiles from each successive position were cross-correlated with the displacement profile from the excitation position. The elastic wave propagation delay was then determined from the maximum of the cross-correlation, and the velocity was obtained from the slope of a linear fit of the elastic wave propagation delays to the corresponding propagation distances. This procedure was repeated for all imaged depths within the tissue, and velocities were averaged depth-wise over 0.2 mm, corresponding to the mucosal layer of the murine colon. This method was also used to monitor the elasticity of the agar basement layer. Since this method of OCE measurement is affected by boundary conditions due to the long wavelength of the elastic wave, we also monitored the elasticity of the agar to ensure consistent results (29,30). The OCE measurements were performed at six positions across the sample as shown in *Figure 1*, and the Young's modulus, *E*, was estimated from the average wave velocity

using the surface wave equation (17,26,31,32),

$$E = \frac{2\rho(1+\upsilon)^3}{(0.87+1.12\upsilon)^2} c_g^2 \quad [1]$$

in which the density of the murine colon was estimated to be ρ=1000 kg/m^3, the Poisson's ratio was assumed to be ν=0.49 for a nearly incompressible tissue, and c_g was the averaged wave velocity for a given sample. While the sample-agar configuration suggests the presence of guided waves, the surface wave equation presents an effective estimate of elastic properties, as shown in our previous work (26). However, future work will account for guided wave velocities and effects of boundary conditions on the elastic wave velocity.

Since the elastic wave is composed of multiple frequencies which travel at different speeds (22), the dispersive behavior of the elastic wave may also provide additional information related to sample biomechanical properties. The dispersion of the elastic wave was quantified by calculating the phase velocity of each frequency in the elastic wave (33). Briefly, the phase shifts of each frequency were obtained by fast Fourier transform (FFT) of the elastic wave vertical temporal displacement profiles. The phase velocities for each frequency were then obtained by linearly fitting the phase delays to the corresponding wave propagation distances for each frequency in the elastic wave (33). The elastic wave dispersion for each group was determined from the average dispersion of each component sample. The elastic wave dispersion curve was linearly fitted to quantify the level of elastic wave dispersion, and the slope of the dispersion curve was utilized as an empirical metric based on the sample biomechanical properties to distinguish the healthy and the colon tissue.

Computational analysis of the tissue optical properties based on the OCT structural image was also performed to distinguish structural changes in the colon tissue. The specific procedure is shown in *Figure 3*, and detailed in our previous work (19,34). Briefly, the OCT intensity A-line (in dB) was linearly fitted, and the slope of the linear fit is used as the first parameter and represents optical attenuation through the sample. The slope of the optical attenuation was removed from the A-line. The standard deviation of the slope-removed A-line was the second tissue structural parameter for disease detection, which reflects the degree of refractive index mismatches within the sample. The third parameter that was used for detecting the diseased tissue was the decay of the slope-removed A-line spatial frequency spectrum. An FFT was performed on the slope-removed A-line. The slope of the linear fit was utilized as an empirical parameter to differentiate the tissues. This method can be useful in detecting texture based variation

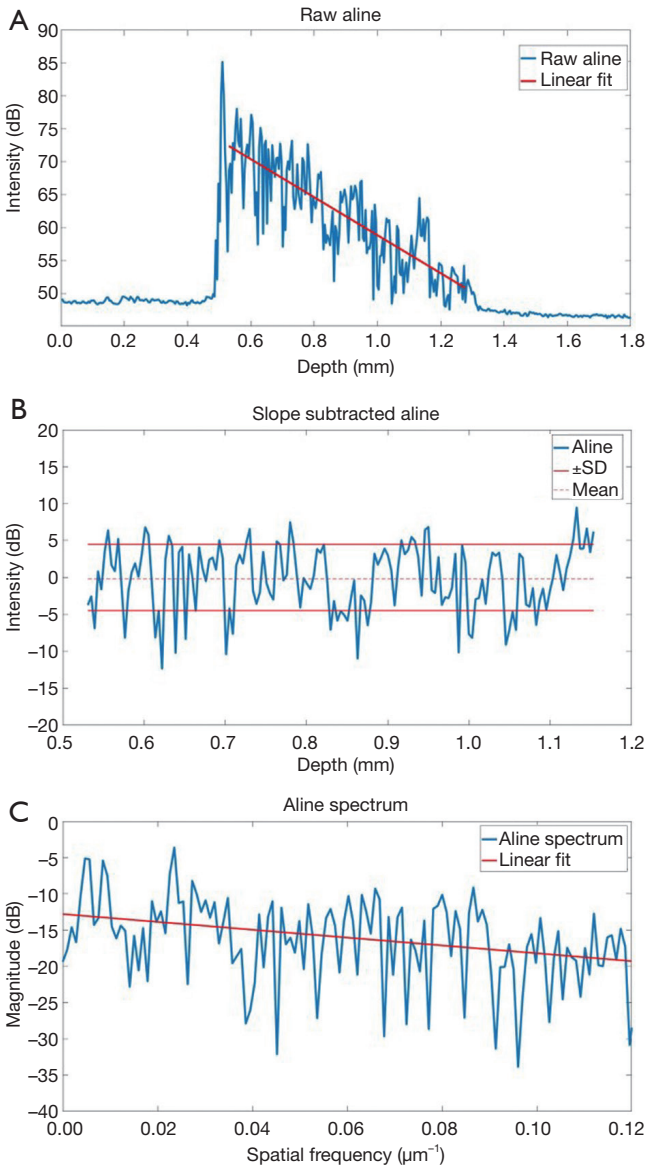

Figure 3 Computational analysis of the OCT signal to determine optical properties of tissues. The computational method used for analyzing OCT signal is shown in *Figure 3*. In (A), the OCT A-line is linearly fitted. The large initial peak indicating surface reflection is ignored. The linear fit is subtracted from the A-line, and the mean and standard deviation are measured and shown in (B). An FFT is used to obtain the spectrum of the slope removed A-line, which is logarithmically scaled in the y-axis and linearly fitted in (C). OCT, optical coherence tomography.

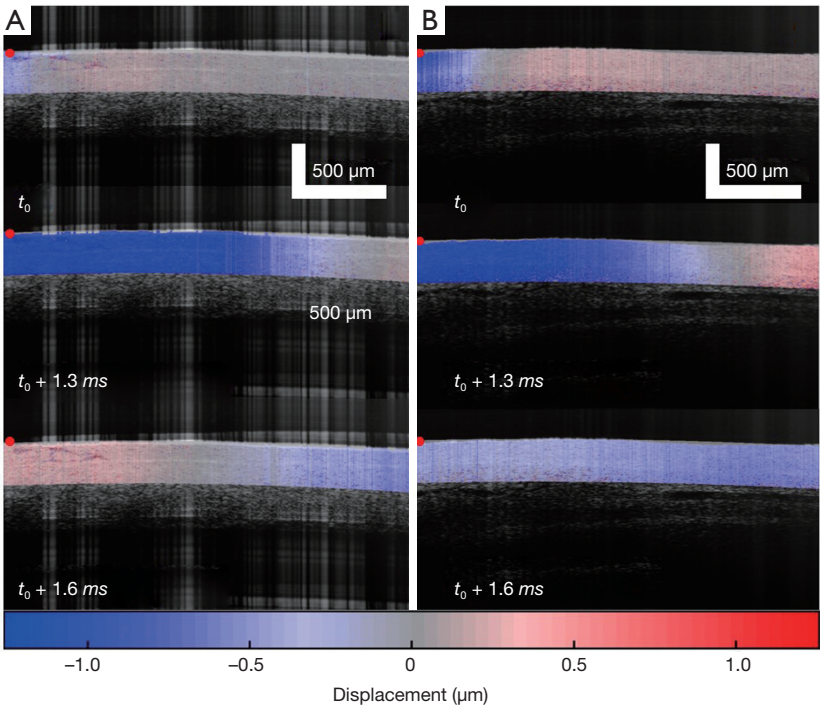

Figure 4 Wave propagation in a control and a colitis sample. *Figure 4* shows the spatio-temporal displacement of an elastic wave in a representative sample from the control group (A), and the DSS-colitis group (B). The elastic wave is induced from the side, indicated by the red dot. Note that over each time point, the elastic wave propagates further in the control sample, suggesting higher stiffness, compared to the colitis sample. Shown data is representative of data obtained from 12 murine colon samples (4 with DSS-colitis and 8 healthy).

and identifying irregularities in tissue that may contribute to the measured OCT signal (35). A lower decay coefficient suggests that there are more low frequency components in the change in tissue refractive index. This computational analysis was performed on the first A-line (out of 1,500 temporal A-lines) of each of the 251 positions acquired at each of the measurement locations for each sample. The average OCT signal slope, standard deviation, and spectral decay was quantified for each sample. For this analysis, the entire visible depth was used.

One of the thirteen samples was removed from analysis due to degradation of the agar basement, which significantly altered OCE measurement. After the OCE measurements, the disease state was unblinded based on diagnosis prior to colon excision, revealing eight control and four diseased samples. Each sample was grouped accordingly based on disease state for statistical analysis.

Results

As summarized in *Figure 1*, the thickness of the samples was measured as 1.45±0.2 and 1.50±0.2 mm for both the control and the colitis group respectively. A two-sample *t*-test shows no statistically significant difference in thickness (P=0.66). The velocity of the air-pulse induced elastic wave was measured in control and colitis-diseased murine colon tissues *ex vivo*. The spatio-temporal displacement maps of the wave propagation in typical control and diseased samples are shown in *Figure 4*. Note the faster propagation in the control tissue, where the blue downward displacement has moved further at the same time after the excitation as compared to the diseased tissue. *Figure 5* shows boxplots of the group velocity and Young's modulus as estimated by the surface wave equation of the control and diseased samples. The boxes correspond to median and interquartile range, the whiskers correspond to one standard deviation, and the small inscribed box is the mean. The mean group velocity of the control samples was 1.8±0.6 m/s, and the group velocity of the diseased samples was 1.3±0.2 m/s, where the error is the inter-sample standard deviation. A two-sample *t*-test for unequal variances showed a significant difference between the two groups (P<0.05). After translating the results to

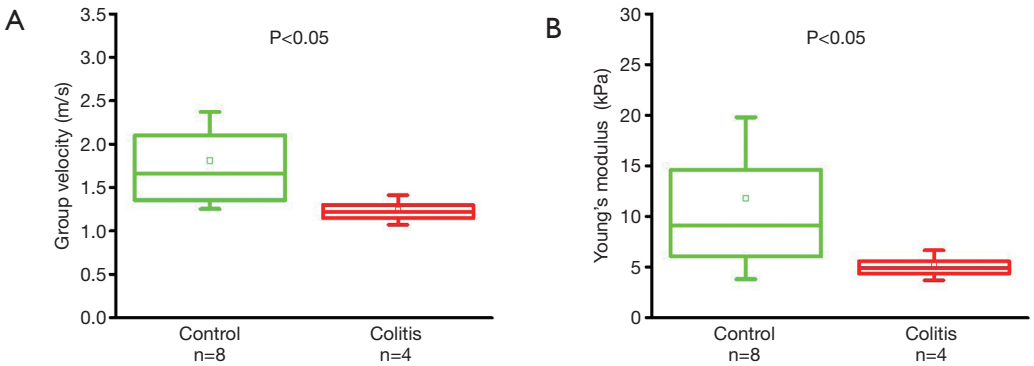

Figure 5 Group velocity and Young's modulus comparison for each tissue group. *Figure 5* shows the group velocity and the Young's modulus estimated by the surface wave equation for each disease group. The box corresponds to the interquartile range, the whiskers correspond to one standard deviation, and the inscribed box reflects the mean. Statistical testing was performed by a two-sample *t*-test for unequal variances.

Young's modulus, the stiffness of the control and colitis samples was 11.8±8.0 and 5.1±1.5 kPa, respectively (P<0.05).

Results of the OCT structural metrics are shown in *Figure 6*. The OCT signal slope for the control and colitis samples was 0.4±0.2 and 0.5±0.2 dB·μm respectively. The standard deviation of the slope removed A-line for the control and colitis samples was 5.8±0.3 and 5.5±0.2 dB. The slope of the spatial frequency decay for the control samples was 92.7±10.0 dB·μm and for the colitis samples was 87.3±4.7 dB·μm. A two-sample *t*-test for unequal variances, revealed statistical significance of P<0.05 respectively for both the standard deviation and the slope of the spatial frequency decay. However, the difference in the signal slope between groups was shown to be statistically insignificant (P=0.64).

Figure 7 shows the average dispersion curve for the control and diseased samples. The slopes of the dispersion curve are noticeably different between the samples—1.5 mm for the healthy samples and 0.8 mm for the colitis samples. The slope of the dispersion curve suggests there is a distinction in biomechanical properties between the control and the diseased samples.

Discussion

Our results demonstrate the potential of OCE to differentiate diseased and healthy colon tissues based on multiple metrics such as stiffness and structural metrics. Though a larger sample size than what is used in this work is needed to ensure that the patterns seen here are consistent and reproducible, our group has shown that a combined approach can significantly improve classification even with a relatively small number of samples (19,34). These results suggest that a two-pronged approach for identifying and distinguishing healthy and UC-diseased tissue using OCE has great promise.

Elasticity calculation was performed over a 0.2 mm depth, corresponding to the mucosal layer. Evaluation of the full tissue mechanical properties is an area of our active future research. One major concern of using the surface wave equation was the thickness of the colon specimens, as the surface wave equation assumes infinite thickness (31,32). Our initial evaluation of the samples prior to OCE measurement did not indicate that samples from either the healthy or diseased groups had distinguishable differences in dimension. As such, while error is likely present in absolute values due to the thickness of the sample, variation in wave speed due to thickness is unlikely to be the distinguishing factor between samples. This same velocity calculation used in this analysis was performed on the several centimeter-thick agar basement layer to monitor the elasticity over time because it was important to ensure that velocity changes to the basement did not affect measurements of the tissue above. Moreover, this method ensured that differences in OCE-assessed stiffness between the diseased and healthy tissues did not originate from differences in tissue thickness or boundary effects. While our previous work has shown that the surface wave equation does provide a reasonable estimate of tissue elasticity from guided waves, it is possible there was an additional error due to the guided wave propagation (29). As such, our measured elasticity highlights relative differences between samples instead of the absolute

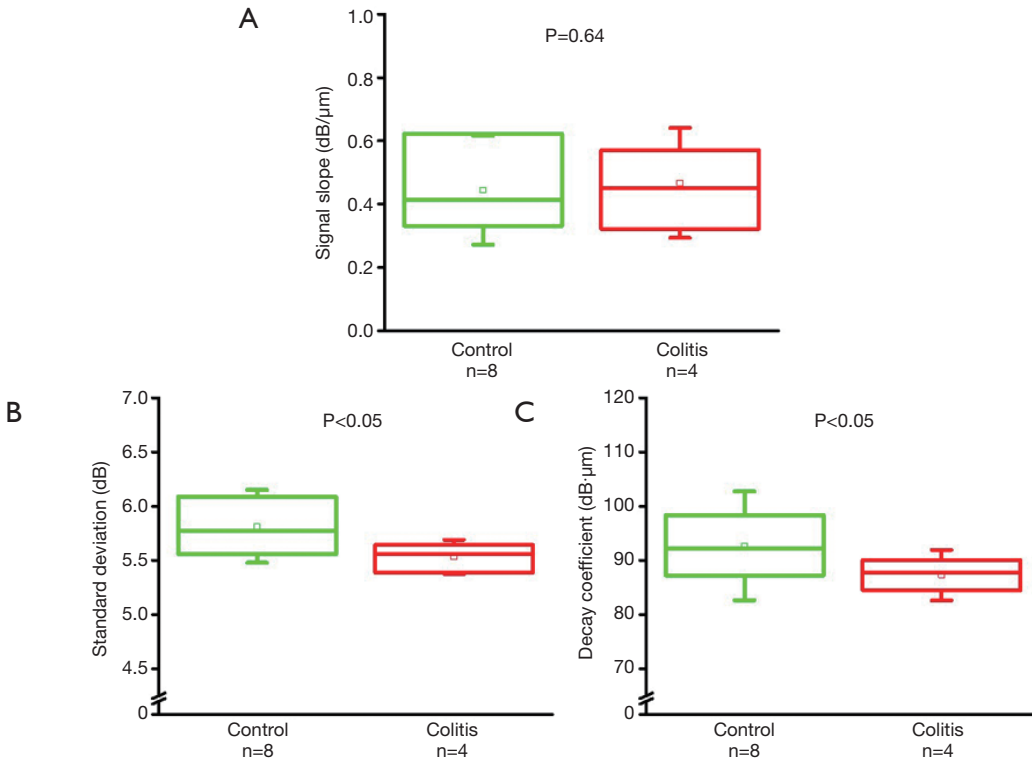

Figure 6 Optical assessment of tissue groups. Optical analysis shown in *Figure 6* suggests that the signal slope of the A-line is indistinct between the two groups. However, the standard deviation of the slope removed A-line and the linear decay coefficient of the A-line indicates that the samples from each disease group can be distinguished. The box corresponds to the interquartile range, the whiskers correspond to one standard deviation, and the inscribed box reflects the mean. Statistical testing was performed by a two-sample *t*-test for unequal variances.

elasticity. Overcoming this limitation is an area of future work.

It has been established that the propagation of a surface wave in a heterogeneous medium will show dispersive behavior, which results in different frequency components of an elastic wave propagating at different velocities (36). Specifically, lower frequency waves (i.e., with longer wavelengths) probe deeper than higher frequency waves (i.e., shorter wavelengths) (29). In the experimental setup utilized, the thin colon tissue was placed on a nutrient agar base, and elastic wave excitation occurs on the surface of the tissue. In this configuration, low frequency components of the surface wave would mostly reflect the elasticity of the lower agar layer, whereas the high frequency components would reflect the elasticity of the top tissue layer (29,30). Under this assumption, the slopes of the dispersion curves suggest a distinct dispersion between each sample group, and that the healthy tissue has greater elastic modulus than the colitis tissue. Initial acute inflammation, which is marked by increased blood flow, tissue fluid accumulation and inflammatory cell infiltration, and later, chronic inflammation marked by increased fibrosis, may impair the elastic properties of the colon differently. These specific differences in histopathology need to be correlated with corresponding OCE readouts, which will be the focus of our future work.

Since the elasticity estimated by the group velocity does not consider this dispersive behavior, phase velocity may provide more robust quantification of sample biomechanical properties. Moreover, the dispersive properties of elastic waves are also heavily influenced by the sample geometry and boundary condition (32). The elastic wave dispersion analysis presented here is by no means comprehensive, and further analysis is necessary to obtain accurate biomechanical properties. Furthermore, the results presented illustrate the average dispersion measured at each position across several specimens within a group, which can introduce significant error. In fact, in the configuration utilized in

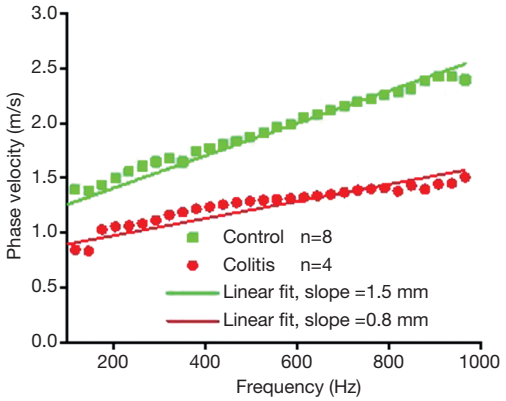

Figure 7 Elastic wave dispersion of each sample group. *Figure* 7 shows the average elastic wave dispersion of each sample group over a frequency range of 1,000 Hz. Standard deviation is not shown for clarity. Note that the phase velocity of the control samples is higher than the colitis samples, suggesting higher stiffness. However, the limited frequency content of the elastic wave induced by air pulse OCE is evident here. OCE, optical coherence elastography.

this work, the slope of the elastic wave dispersion curve is likely additionally affected by the presence of guided waves, sample geometry, and boundary conditions. However, the diseased and healthy tissues were distinguished by their biomechanical properties, and more accurate quantification of tissue biomechanical properties with a more appropriate wave model is possible. Previous work has utilized spectral decomposition to identify layers of differing stiffness (37), but there has yet to be demonstration of a model of wave propagation in a multi-layer medium and its application in OCE. Hence, we are currently developing a multi-layer model that can correctly integrate sample geometry and measurement conditions to provide truly quantitative, and potentially depth-resolved, biomechanical assessment of tissues similar to our previous work in cornea (38). As previously mentioned, since low frequency waves describe the elasticity of a large sample area, and high frequency waves describe the sample surface, an alternative method to more accurately characterize the tissue in the sample-agar configuration shown in this work is to induce elastic waves with higher frequency content. This method would overcome a limitation of air pulse OCE, increase the spatial resolution, and minimize the influence of boundary conditions. Furthermore, we have demonstrated the potential utility of techniques such as nanobomb OCE (39), that are capable of producing elastic waves with frequency content in the tens of kilohertz, which would be sufficient for high-resolution elastography of thin murine colons. On the other hand, compression OCE has been shown to be highly effective for spatially mapping the biomechanical properties of tissues (17,40). The imaging depth in compression OCE may be limited, but this method may provide an effective tool for identifying the disease margins of colorectal pathologies with high-resolution and sensitivity, as has been shown in breast tissue (40).

Optical analysis demonstrated that the OCT signal slope which represents optical attenuation through the sample, suggests that the control and colitis tissue are not distinguishable by attenuation. However, a distinct variation was present in the refractive index mismatches along tissue depth, which reflects the differences in tissue microstructure between the healthy and diseased colon tissue. Considering that UC is known to present as inflammation, scarring, and ulceration over extensive stretches of the colon tissue, the differences in the optical properties were expected. However, further analysis is needed to identify the pathological basis of this result, such as histological analysis across different regions of the diseased colon. This would help pinpoint the specific morphological changes in the colon tissue that correspond to the changes in optical parameters measured by OCT. Additionally, samples were highly scattering, and it was not possible to image through the entire sample. This limits analysis to the visible depth of the colon tissue and introduces potential bias since various anatomical sections of the tissue may have had slightly different thicknesses between samples. Analyzing the tissue optical properties for each layer of the colon tissue is the next step of our image analysis. Furthermore, detailed analysis of the OCT signal to obtain estimates of sample attenuation has been shown (41) as well as higher resolution OCT techniques and computational analyses (42) and texture-based analysis (43). Multiple scattering events in depth through the tissue may also cause variations in the measured optical properties, and several measures have been suggested to account for these events (44-46). Future work will evaluate the effectiveness of these measures as additional parameters for more accurate detection of disease even though scattering dominated the OCT signal.

In this work, we utilized a combined optical and biomechanical assessment of murine colon tissue to detect DSS-induced UC. While this two-pronged method could be very useful for characterizing tissue, each separate technique has its own limitations that restrict their combined effectiveness. One significant challenge in OCE

is depth-wise characterization of mechanical properties and the low spatial resolution of low frequency elastic waves. The colon is made of several layers, but biomechanical evaluation of each of these structures can be challenging, due to the limited resolution of air puff OCE (17). The tissue-agar configuration in this work further extends this limitation, due to the boundary condition that the agar basement introduces. Additionally, OCE resolution is inherently dependent on the excitation technique, reconstruction method, mechanical contrast, and is generally inferior to the resolution of its parent imaging modality OCT (18,26). On the other hand, one significant limitation of OCT in this work arises from the highly scattering nature of the colon tissue; the entire tissue depth is not visible in the OCT image. As such, analysis of optical properties may be prone to bias due to the varying visible depths between samples. Additionally, the OCT signal slope is sensitive to changes between interfaces, which could occur in multi-layered tissue (34). Both OCE and OCT have individual limitations and sources of error that may combine constructively or destructively, which need to be explored further.

Even though the number of samples was limited in this work, the results demonstrate the potential of OCE as a detection technique for IBD, including UC and Crohn's disease. However, more work is needed to develop excitation techniques and quantitative and analytical methods to accurately quantify the viscoelasticity of the colon tissue. Nevertheless, imaging a larger number of samples and performing correlative analyses with clinically-established assessments of disease severity, such as Disease Activity Index score and Macroscopic Disease Activity score is needed. Moreover, the samples in this work were extracted, and we are currently developing probe-based OCE techniques for *in situ* and *in vivo* studies (47).

In summary, we have demonstrated the potential of air-pulse OCE to differentiate healthy and colitis-diseased murine colon tissue exhibiting lesions that are very similar to human IBD (20). Initial estimates of tissue stiffness based on group velocity indicated that healthy tissue was stiffer than diseased tissue. Analysis of the dispersive behavior of the samples also suggested higher stiffness of the healthy tissue, but also a possible increased viscosity. Moreover, structural analysis of the tissue demonstrated a distinct difference in tissue optical properties between the healthy and colitis-diseased tissue. The results raise hope that OCE may be useful for detecting IBD and possibly other colorectal pathologies.

Acknowledgments

Funding: This work was supported, in part, by NIH grants 2R01EY022362, 1R01HL130804, and 1R21CA231561.

Footnote

Conflicts of Interest: The authors have no conflicts of interest to declare.

Ethical Statement: All procedures were performed under an approved protocol by the University of Houston Institutional Animal Care and Use Committee.

References

1. Kappelman MD, Rifas-Shiman SL, Kleinman K, Ollendorf D, Bousvaros A, Grand RJ, Finkelstein JA. The prevalence and geographic distribution of Crohn's disease and ulcerative colitis in the United States. Clin Gastroenterol Hepatol 2007;5:1424-9.
2. Eaden JA, Abrams KR, Mayberry JF. The risk of colorectal cancer in ulcerative colitis: a meta-analysis. Gut 2001;48:526.
3. Ng SC, Shi HY, Hamidi N, Underwood FE, Tang W, Benchimol EI, Panaccione R, Ghosh S, Wu JCY, Chan FKL, Sung JJY, Kaplan GG. Worldwide incidence and prevalence of inflammatory bowel disease in the 21st century: a systematic review of population-based studies. Lancet 2018;390:2769-78.
4. Benchimol EI, Bernstein CN, Bitton A, Carroll MW, Singh H, Otley AR, Vutcovici M, El-Matary W, Nguyen GC, Griffiths AM, Mack DR, Jacobson K, Mojaverian N, Tanyingoh D, Cui Y, Nugent ZJ, Coulombe J, Targownik LE, Jones JL, Leddin D, Murthy SK, Kaplan GG. Trends in Epidemiology of Pediatric Inflammatory Bowel Disease in Canada: Distributed Network Analysis of Multiple Population-Based Provincial Health Administrative Databases. Am J Gastroenterol 2017;112:1120-34.
5. Rameshshanker R, Arebi N. Endoscopy in inflammatory bowel disease when and why. World J Gastrointest Endosc 2012;4:201-11.
6. Ellrichmann M, Wietzke-Braun P, Dhar S, Nikolaus S, Arlt A, Bethge J, Kuehbacher T, Wintermeyer L, Balschun K, Klapper W, Schreiber S, Fritscher-Ravens A. Endoscopic ultrasound of the colon for the differentiation of Crohn's disease and ulcerative colitis in comparison with healthy controls. Aliment Pharmacol Ther 2014;39:823-33.

7. Panés J, Bouzas R, Chaparro M, Garcia-Sanchez V, Gisbert JP, Martinez de Guerenu B, Mendoza JL, Paredes JM, Quiroga S, Ripolles T, Rimola J. Systematic review: the use of ultrasonography, computed tomography and magnetic resonance imaging for the diagnosis, assessment of activity and abdominal complications of Crohn's disease. Aliment Pharmacol Ther 2011;34:125-45.
8. Dhar A, Johnson KS, Novelli MR, Bown SG, Bigio IJ, Lovat LB, Bloom SL. Elastic scattering spectroscopy for the diagnosis of colonic lesions: initial results of a novel optical biopsy technique. Gastrointest Endosc 2006;63:257-61.
9. Watanabe O, Ando T, Maeda O, Hasegawa M, Ishikawa D, Ishiguro K, Ohmiya N, Niwa Y, Goto H. Confocal endomicroscopy in patients with ulcerative colitis. J Gastroenterol Hepatol 2008;23 Suppl 2:S286-90.
10. Li T, Hui H, Hu C, Ma H, Yang X, Tian J. Multiscale imaging of colitis in mice using confocal laser endomicroscopy, light-sheet fluorescence microscopy, and magnetic resonance imaging. SPIE, 2019.
11. Tsai T-H, Leggett CL, Trindade AJ, Sethi A, Swager A-F, Joshi V, Bergman JJ, Mashimo H, Nishioka NS, Namati E. Optical coherence tomography in gastroenterology: a review and future outlook. J Biomed Opt 2017;22:1-17.
12. Li Y, Snedeker JG. Elastography: modality-specific approaches, clinical applications, and research horizons. Skeletal Radiol 2011;40:389-97.
13. Jugé L, Doan BT, Seguin J, Albuquerque M, Larrat B, Mignet N, Chabot GG, Scherman D, Paradis V, Vilgrain V, Van Beers BE, Sinkus R. Colon tumor growth and antivascular treatment in mice: complementary assessment with MR elastography and diffusion-weighted MR imaging. Radiology 2012;264:436-44.
14. Giannetti A, Biscontri M, Matergi M. Feasibility of real-time strain elastography in colonic diseases. J Ultrasound 2014;17:321-30.
15. Ishikawa D, Ando T, Watanabe O, Ishiguro K, Maeda O, Miyake N, Nakamura M, Miyahara R, Ohmiya N, Hirooka Y, El-Omar EM, Goto H. Images of colonic real-time tissue sonoelastography correlate with those of colonoscopy and may predict response to therapy in patients with ulcerative colitis. BMC Gastroenterol 2011;11:29.
16. Schmitt J. OCT elastography: imaging microscopic deformation and strain of tissue. Opt Express 1998;3:199-211.
17. Larin KV, Sampson DD. Optical coherence elastography - OCT at work in tissue biomechanics [Invited]. Biomed Opt Express 2017;8:1172-202.
18. Hepburn MS, Wijesinghe P, Chin L, Kennedy BF. Analysis of spatial resolution in phase-sensitive compression optical coherence elastography. Biomed Opt Express 2019;10:1496-513.
19. Liu CH, Du Y, Singh M, Wu C, Han Z, Li J, Chang A, Mohan C, Larin KV. Classifying murine glomerulonephritis using optical coherence tomography and optical coherence elastography. J Biophotonics 2016;9:781-91.
20. Okayasu I, Hatakeyama S, Yamada M, Ohkusa T, Inagaki Y, Nakaya R. A novel method in the induction of reliable experimental acute and chronic ulcerative colitis in mice. Gastroenterology 1990;98:694-702.
21. Wang S, Larin KV. Shear wave imaging optical coherence tomography (SWI-OCT) for ocular tissue biomechanics. Opt Lett 2014;39:41-4.
22. Deffieux T, Montaldo G, Tanter M, Fink M. Shear Wave Spectroscopy for In Vivo Quantification of Human Soft Tissues Visco-Elasticity. IEEE Trans Med Imaging 2009;28:313-22.
23. Walldorf J, Hermann M, Porzner M, Pohl S, Metz H, Mader K, Zipprich A, Christ B, Seufferlein T. In-vivo monitoring of acute DSS-Colitis using Colonoscopy, high resolution Ultrasound and bench-top Magnetic Resonance Imaging in Mice. Eur Radiol 2015;25:2984-91.
24. Li J, Wang S, Manapuram RK, Singh M, Menodiado FM, Aglyamov S, Emelianov S, Twa MD, Larin KV. Dynamic optical coherence tomography measurements of elastic wave propagation in tissue-mimicking phantoms and mouse cornea in vivo. J Biomed Opt 2013;18:121503.
25. Wang S, Larin KV, Li J, Vantipalli S, Manapuram RK, Aglyamov S, Emelianov S, Twa MD. A focused air-pulse system for optical-coherence-tomography-based measurements of tissue elasticity. Laser Phys Lett 2013;10:075605.
26. Han Z, Li J, Singh M, Wu C, Liu CH, Wang S, Idugboe R, Raghunathan R, Sudheendran N, Aglyamov SR, Twa MD, Larin KV. Quantitative methods for reconstructing tissue biomechanical properties in optical coherence elastography: a comparison study. Phys Med Biol 2015;60:3531-47.
27. Song S, Huang Z, Wang RK. Tracking mechanical wave propagation within tissue using phase-sensitive optical coherence tomography: motion artifact and its compensation. J Biomed Opt 2013;18:121505.
28. Wang S, Larin KV. Optical coherence elastography for tissue characterization: a review. J Biophotonics

2015;8:279-302.
29. Mohan KD, Oldenburg AL. Elastography of soft materials and tissues by holographic imaging of surface acoustic waves. Opt Express 2012;20:18887-97.
30. Aglyamov SR, Wang S, Karpiouk AB, Li J, Twa M, Emelianov SY, Larin KV. The dynamic deformation of a layered viscoelastic medium under surface excitation. Phys Med Biol 2015;60:4295-312.
31. Graff KF. Wave Motion in Elastic Solids. Dover Publications, 2012.
32. Doyle JF. Wave Propagation in Structures Spectral Analysis Using Fast Discrete Fourier Transform. New York: Springer; 1997.
33. Wang S, Larin KV. Noncontact depth-resolved micro-scale optical coherence elastography of the cornea. Biomed Opt Express 2014;5:3807-21.
34. Wang S, Liu CH, Zakharov VP, Lazar AJ, Pollock RE, Larin KV. Three-dimensional computational analysis of optical coherence tomography images for the detection of soft tissue sarcomas. J Biomed Opt 2014;19:21102.
35. Somfai GM, Tátrai E, Laurik L, Varga BE, Ölvedy V, Smiddy WE, Tchitnga R, Somogyi A, DeBuc DC. Fractal-based analysis of optical coherence tomography data to quantify retinal tissue damage. BMC Bioinformatics 2014;15:295.
36. Li C, Huang Z, Wang RK. Elastic properties of soft tissue-mimicking phantoms assessed by combined use of laser ultrasonics and low coherence interferometry. Opt Express 2011;19:10153-63.
37. Li C, Guan G, Cheng X, Huang Z, Wang RK. Quantitative elastography provided by surface acoustic waves measured by phase-sensitive optical coherence tomography. Opt Lett 2012;37:722-4.
38. Han Z, Li J, Singh M, Wu C, Liu C-H, Raghunathan R, Aglyamov SR, Vantipalli S, Twa MD, Larin KV. Optical coherence elastography assessment of corneal viscoelasticity with a modified Rayleigh-Lamb wave model. J Mech Behav Biomed Mater 2017;66:87-94.
39. Liu CH, Nevozhay D, Schill A, Singh M, Das S, Nair A, Han Z, Aglyamov S, Larin KV, Sokolov KV. Nanobomb optical coherence elastography. Opt Lett 2018;43:2006-9.
40. Kennedy KM, Chin L, McLaughlin RA, Latham B, Saunders CM, Sampson DD, Kennedy BF. Quantitative micro-elastography: imaging of tissue elasticity using compression optical coherence elastography. Sci Rep 2015;5:15538.
41. Scolaro L, McLaughlin RA, Klyen BR, Wood BA, Robbins PD, Saunders CM, Jacques SL, Sampson DD. Parametric imaging of the local attenuation coefficient in human axillary lymph nodes assessed using optical coherence tomography. Biomed Opt Express 2012;3:366-79.
42. Alexandrov SA, Subhash HM, Zam A, Leahy M. Nano-sensitive optical coherence tomography. Nanoscale 2014;6:3545-9.
43. Lindenmaier AA, Conroy L, Farhat G, DaCosta RS, Flueraru C, Vitkin IA. Texture analysis of optical coherence tomography speckle for characterizing biological tissues in vivo. Opt Lett 2013;38:1280-2.
44. Wang RK. Signal degradation by multiple scattering in optical coherence tomography of dense tissue: a Monte Carlo study towards optical clearing of biotissues. Phys Med Biol 2002;47:2281-99.
45. Karamata B, Laubscher M, Leutenegger M, Bourquin S, Lasser T, Lambelet P. Multiple scattering in optical coherence tomography. I. Investigation and modeling. J Opt Soc Am A Opt Image Sci Vis 2005;22:1369-79.
46. Kirillin MY, Priezzhev AV, Myllylä R. Role of multiple scattering in formation of OCT skin images. Quantum Electronics 2008;38:570-5.
47. Karpiouk AB, VanderLaan DJ, Larin KV, Emelianov SY. Integrated optical coherence tomography and multielement ultrasound transducer probe for shear wave elasticity imaging of moving tissues. J Biomed Opt 2018;23:1-7.

Cite this article as: Nair A, Liu CH, Singh M, Das S, Le T, Du Y, Soomro S, Aglyamov S, Mohan C, Larin KV. Assessing colitis *ex vivo* using optical coherence elastography in a murine model. Quant Imaging Med Surg 2019;9(8):1429-1440. doi: 10.21037/qims.2019.06.03

